



Load–Displacement Behavior of Driven Piles in Sand Using CPT-Based Stress and Strain Fields

Fatemeh Valikhah¹ · Abolfazl Eslami¹ · Mehdi Veiskarami²

Received: 24 September 2018 / Revised: 24 November 2018 / Accepted: 10 December 2018 / Published online: 21 December 2018
© Iran University of Science and Technology 2019, Corrected publication 2019

Abstract

The bearing capacity of piles is often estimated by a variety of methods such as the limit equilibrium or the limit analysis. In contrast, the load–displacement behavior, which should not be disregarded in common practices, cannot be obtained as simply as the bearing capacity. The reason is its dependency on the stress and the strain (or the displacement) fields around the pile. In the current work, attempt has been made to predict the load–displacement behavior of driven piles in sand by direct and indirect implementation of the cone penetration test (CPT) data into the displacement field. CPT often serves as a very successful in situ test which provides a close link between the soil resistance and the bearing capacity, although it brings no direct information. A rather simple procedure is presented to indirectly use the CPT data to find the stress and strain fields. While the pattern of the failure mechanism has been obtained by the method of stress characteristics, the displacement (and strain) field has been found by the kinematics of the failure mechanism. The proposed procedure has been calibrated and verified by 98 case histories including pile load test results in conjunction with CPT data. Comparisons made by this new method show that the CPT-based method of stress characteristics can be successfully used in load–displacement prediction of driven piles.

Keywords Pile · CPT · Load–displacement · Stress characteristics method · Displacement field

1 Introduction

Estimation of the bearing capacity of piles has been always a challenging issue for geotechnical engineers due to inherently complex behavior of soil, relatively long length extending into a variety of soil layers, deep embedment depth and soil–pile interaction. There are several different methods to estimate the bearing capacity of piles: (a) static analysis methods, (b) direct and indirect use of in situ test results, (c) static load test and (d) dynamic methods [1, 2].

Studies show that the bearing capacity may be far different from the reality if the deformations are neglected [3]. In addition, unless under ideal conditions, such as a rigid-perfectly plastic materials, there is no precise and unique definition of limit load for footings and piles. As a consequence, the bearing capacity and load–displacement analysis should be accomplished simultaneously, or, in other words, the first should be determined from the second. The load–displacement behavior of piles is often obtained by conducting a pile load test which is very costly and time consuming; or by complicated finite element modeling, which in turn requires a great deal of effort to properly define the soil properties to be considered in the analysis. There are also some simplified methods primarily based on statistical observations ($t - \zeta$ and $q - \zeta$ curves) which are only rough estimates to obtain satisfactory results.

In this study, a semi-analytical method with a theoretical basis based on a universally accepted and commonly used field test (cone penetration test, CPT) has been proposed. For this purpose, the CPT data, as a very useful tool due to its repeatability, accuracy and continuity of the records [4, 5] has been employed. The procedure comprises three different

✉ Abolfazl Eslami
afeslami@aut.ac.ir

Fatemeh Valikhah
fvalikhah@aut.ac.ir

Mehdi Veiskarami
mveiskarami@gmail.com; mveiskarami@shirazu.ac.ir

¹ School of Civil and Environmental Engineering, Amirkabir University of Technology, Tehran, Islamic Republic of Iran

² Department of Civil and Environmental Engineering, Shiraz University, Shiraz, Islamic Republic of Iran

ingredients. First, a displacement field is constructed based on an adopted failure mechanism and fundamental requirements of the limit analysis. Then, the strain field is calculated which is nothing but the symmetric part of the gradient of the displacement field. Finally, the soil shear strength is assumed to be a function of the maximum shear strain and the residual shear resistance of the soil which is a legitimate assumption. This relationship can be found by direct and/or indirect use of CPT data based on which, the residual shear strength of the soil can be found. The strain field is then updated by further penetration of the pile into the soil and as a consequence, the stress field and the boundary load at the pile tip will be calculated. This procedure will provide a complete load–displacement curve of the pile. The results are verified with experimental data obtained from pile load test data available in the literature. In addition, further comparisons have been made with various methods based on the cone penetration test (CPT) data.

In what comes next, a brief review of the theory behind the procedure and a literature review is presented and afterwards, the procedure will be explained in detail with numerical results and comparisons.

2 Behind the Theory

2.1 Bearing Capacity of Driven Piles by CPT Records

In view of the wide range of methods and equipments now available in regard with the analysis, design and construction of deep foundations, a thorough geotechnical study is very reliable and nowadays, at hand, for most engineering projects. They also obviate any further need for laboratory tests which are often conducted on disturbed samples from discrete locations. In particular when a deep foundation is analyzed, in situ tests can be much efficiently used to perform a precise analysis. Among many in situ tests developed in the recent years, CPT resembles a pile under axial load which can be used as a model pile for both analysis and design [6, 7]. The CPT is basically developed for soft clays [8] and its application in very compacted sand and coarsely granular materials is limited. However, it can be used in loose to medium sands as well as most fine sands [9], which is the target soil in this paper.

The studies on the actual cases show that the toe and shaft resistance of piles are not the exact values of tip and sleeve resistances recorded by CPT, due to the scale differences between pile and CPT and also the stress level. The scale effects include the geometry, the rate of pile and CPT penetration in soil. The stress level is also a consequence of scale and the level of transmitted loads from the pile to the surrounding soil. Consequently, the deformation generated in soil in effect of CPT penetration is much higher than the one in effect of pile

penetration. The soil fails during CPT penetration, however, it may not occur during the pile driving. As a result, the mobilized resistance along the CPT and the pile is different which is not considered in current CPT-based methods.

In this study, an analytical–numerical study has been conducted to estimate the bearing capacity and axial load–displacement behavior of driven piles in granular soils using CPT records. The ingredients of the computational procedure and assumptions behind it are presented in the next sections.

2.2 Stress Characteristics Method

The method of stress characteristics or the slip lines method is known as a standard method in solving some plasticity or stability problems in soils, which is often attributed to Sokolovski during 1960s [10]. This method was then developed and applied to many problems such as the complex bearing problem and extended to a variety of considerations. Among them, Martin and Houlsby [11] applied the slip line method for the bearing capacity estimation of the spudcan foundations under combined loading. Kumar [12] used the stress characteristics method to investigate the effect of footing roughness on the bearing capacity of foundations. Veiskarami et al. [13] implemented the slip line method to analyze the end-bearing capacity of driven piles in sands. Recently, Veiskarami et al. [14, 15] studied the effect of flow rule on the bearing capacity of strip foundations on sand by a new method composed of the stress characteristics together with the kinematic approach of the upper-bound limit analysis. These latter contributions are important as they are central to finding the displacement field of the current research.

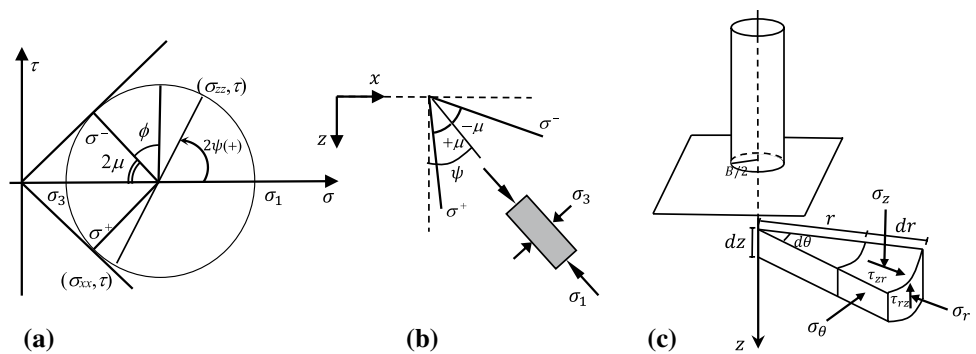
The bearing capacity of foundations can be obtained by this method where both the equilibrium and yield equations are satisfied along the so-called slip line directions, simultaneously. Since these equations are transformed into ordinary differential equations along the slip lines, this method was also given the name of the “method of stress characteristics”.

The Mohr stress circle is a useful graphical tool to visualize the characteristics directions. The finite difference method can be used to solve these equations simultaneously which has been well-described in the literature [16, 17]. The equilibrium equations, in absence of lateral body forces, in cylindrical coordinates system, with axial symmetry, in terms of coordinates, r , θ and z , which are shown in Fig. 1, can be written as follows:

$$\begin{cases} \frac{\partial \sigma_r}{\partial r} + \frac{\partial \tau_{rz}}{\partial z} + \frac{\sigma_r - \sigma_\theta}{r} = 0 \\ \frac{\partial \sigma_z}{\partial z} + \frac{\partial \tau_{rz}}{\partial r} + \frac{\tau_{rz}}{r} = \rho \gamma_w \end{cases} \quad (1)$$

where σ_r , σ_z , σ_θ and τ_{rz} are components of stress tensor, $\rho \gamma_w$ is the body force along the z direction. According to Larkin [18] the direction of the major principal stress with

Fig. 1 **a** Mohr stress circle and the directions of slip lines; **b** the directions of slip lines with respect to principal stresses and **c** cylindrical coordinate system and stress components



z direction, is denoted by an angle ψ and the mean stress by σ . Employing the Mohr–Coulomb yield criterion, i.e., $\tau = \sigma \tan \phi + c$, with c and ϕ as soil shear strength parameters, the stress state can be fully defined as follows [16]:

$$\sigma_r = \sigma(1 - \sin \phi \cos 2\psi) \tag{2a}$$

$$\sigma_z = \sigma(1 + \sin \phi \cos 2\psi) \tag{2b}$$

$$\sigma_\theta = \sigma_3 = \sigma(1 - \sin \phi) \tag{2c}$$

$$\tau_{rz} = \sigma \sin \phi \sin 2\psi. \tag{2d}$$

The equilibrium and yield equations can be combined together to find the stress characteristics equations. The system of equations found in this way can be then solved by the method of stress characteristics. The equations are as follows:

Along the positive (σ^+) and the negative (σ^-) stress characteristics:

$$\frac{dr}{dz} = \tan(\psi \pm \mu), \tag{3}$$

$$d\sigma \cos \phi \pm 2\sigma \sin \phi d\psi + \frac{\sigma}{r} [\sin \phi \cos \phi dr \pm (\sin^2 \phi - \sin \phi) dz] = \mp \rho \gamma_w (\sin \phi dr - \cos \phi dz), \tag{4}$$

where $\mu = \pi/4 - \phi/2$. Figure 1 shows the definition of parameters involved in these equations.

As it is known, the installation of a driven pile is different from the CPT sounding process. Hence, this discrepancy should be taken into account and addressed in predicting the load-settlement behavior of driven piles, since the CPT data just gives the in situ information of the stratum. For this purpose, the driving effect is considered on the model boundary conditions by definition of a passive lateral earth pressure along the pile shaft. In other words, the driven piles, often called displacement piles, can move the soil away and put it into the passive state during the driving process. Of course this is a limiting condition and the complete passive force may

not be mobilized completely in practice. However, such an assumption more or less complies better with the actual condition.

2.2.1 Non-Associated Flow Rule

The influence of flow rule is very important in estimation of the limit load based on plasticity theory. The angle of dilation reduces as the shear strains develop and it affects both the pattern of failure mechanism and the limit load. One should note that the limit load in the context of the limit analysis in perfectly plastic materials does not depend on the type of flow rule. However, the limit load obtained by a kinematically admissible failure mechanism depends on the geometry of the failure pattern which in turn depends on the flow rule. Non-associated materials exhibit a smaller failure pattern and a lower limit load. Therefore, the angle of dilation, as a measure of non-associativity, affects the failure pattern and the limit load.

An associated flow rule, as in many methods, is the basis of the stress characteristics method and most limit load theorems. It is conventional to find the solution based on an associated flow rule assumption but in fact, a non-associated flow rule governs the actual behavior of most geomaterials. Therefore, the non-associativity should be taken into account if an appropriate estimation of the bearing capacity is required. To include the influence of the flow rule, one significant step was taken by Drescher and Detournay [19] in computing equivalent values for soil cohesion and friction angle in case of a non-associated flow rule. Equivalent values can be computed by the following equations derived independently by Davis [20] and Rowe [21] based on equating the rate of plastic work for a non-associative and an equivalently associative material:

$$\tan \phi^* = \eta \tan \phi, \tag{5}$$

$$c^* = \eta c, \tag{6}$$

$$\eta = \frac{\cos \nu \cos \phi}{1 - \sin \nu \sin \phi}. \tag{7}$$

In these equations, ν is the soil angle of dilation, ϕ is actual friction angle, c is cohesion, c^* is the modified (or

equivalent) cohesion due to non-associativeness and ϕ^* is the modified (or equivalent) friction angle for spotting the non-associativity of soils.

Studies show that the equivalent shear strength terms do not change significantly when the dilation angle is around 0.5ϕ and smaller. In addition, for the bearing capacity problems, the shear strains are often high enough to reach a residual strength corresponding to very low volume change and very small dilation angles. Therefore, due mainly to rather very high shear deformations and very low dilation angles mobilized in the soil around a pile, the dilation angle is conservatively assumed to be $\nu = 0.1\phi$.

2.3 Soil Strength Parameter by Use of CPT Records

In this study, the shear strength parameter of soil (ϕ), which is used as an input data for numerical modeling have been estimated first by the indirect use of CPT data. The results of equations presented by Robertson and Campanella [9], Bowles [22] and Kulhawy and Mayne [23] mentioned in Table 1 are investigated. The geometric cone resistance has been averaged over three different zones, i.e., $2b$ below the cone tip (b is the pile diameter) and $4b$ above (i.e., $2b/4b$), $3b/6b$ and $4b/8b$ are calculated to see which averaging method gives better estimations. From these zones, the zone $4b/8b$ (i.e., averaging over a zone extended from $4b$ below the cone tip to $8b$ above the tip) and the equation presented by Kulhawy and Mayne [23] are found to be more appropriate.

3 Compiled Database

A database of case histories from the results of 98 full-scale pile load tests is recompiled with complete information on the soil type and the results of CPT soundings performed close to the pile locations. The cases were obtained

from nine different sources. Forty case studies are used for calibration and fifty-eight cases for verification of the proposed approach. Tables 2 and 3 summarize these cases with reference to the soil and the pile characteristics.

All piles are of “driven pile” type. Most of cases are in sand and some in silt and mixed soils. The shapes of piles are octagonal, square, round and pipe (opened and closed ended). The open-ended piles are assumed to be fully plugged. The pile width varies between 73 and 915 mm and the pile length between 3.44 and 67 m. Pile materials are concrete (with rather rough interface) or steel (with rather smooth interface).

4 Proposed Approach

Studies show that the response of a pile to an applied axial load can not be considered as the pile ultimate capacity, but it is a function of stress and strain conditions around the pile [3]. Therefore, it is necessary to simultaneously analyze the bearing capacity and the load–displacement response of pile.

Prediction of the load–displacement response of piles is often a difficult task. The pile load test is considered to be one of the most reliable methods for prediction of the load–displacement response. However, this test is both time consuming and expensive. Alternatively, it is more advantageous to develop simple analytical or numerical methods based on rather limited test results.

In this study, a new analytical–numerical method is proposed to estimate the bearing capacity and load–displacement behavior of axially loaded piles based on CPT records. The method of stress characteristics is used to obtain the stress field around the pile and the kinematics of the deformation (i.e., the failure pattern) has been also determined.

4.1 Stress Field from the Slip Lines Method

When the static analysis method is used, the failure mechanism around the pile tip or the shaft, should be either assumed, or, found naturally. For example, in methods based on the limit equilibrium or the upper bound limit analysis, the failure mechanism is assumed a priori. Whereas, in methods such as the lower bound limit analysis or the stress fields methods, it is obtained naturally.

Therefore, the actual stress field is first determined by the method of stress characteristics where the yield equation is satisfied, which is the initial failure pattern formed around the pile. Then, the failure mechanism is progressively extended by a hardening soil model and the plastic strains are developed in the soil around the pile. The concept is

Table 1 Relations between ϕ and q_c

No.	Equation	References	Remarks
1	$\phi = \arctan \left(0.1 + 0.38 \log \left(\frac{q_c}{\sigma'_v} \right) \right)$	[9]	q_c : Cone tip resistance (kPa) σ'_v : Effective overburden stress (kPa)
2	$\phi = 17.6 + 11 \log \frac{q_c}{\sqrt{100 \sigma'_v}}$	[22]	q_c is in kPa
3	Sand $\phi = 29 + \sqrt{q_c}$ Gravel $\phi = 29 + \sqrt{q_c} + 5$ Silty sand $\phi = 29 + \sqrt{q_c} - 5$	[23]	q_c is in MPa

Table 2 Case study records for calibration

No.	Refs.	Soil type	Pile shape	Material	L (m)	b (mm)	G.W.T (m)	q_c (MPa)	f_s (MPa)
1	[24]	Sand	Pipe (closed)	Steel	19.24	457	4	1.68	0.01
2		Sand	Pipe (closed)	Steel	19.37	457	4	18.24	0.08
3		Sand	Pipe (closed)	Steel	19.05	457	4	11.9	0.1
4		Sand	Pipe (closed)	Steel	18.9	457	4	13.74	0.14
5	[25]	Sand	Pipe (closed)	Steel	9.1	73	0.5	2.5	0.02
6		Sand	Pipe (closed)	Steel	9.1	88.9	0.5	2.5	0.02
7		Sand	Pipe (closed)	Steel	9.1	114.3	0.5	2.5	0.02
8		Sand	Pipe (open)	Steel	9.1	73	0.5	2.5	0.02
9		Sand	Pipe (open)	Steel	9.1	88.9	0.5	2.5	0.02
10		Sand	Pipe (open)	Steel	9.1	114.3	0.5	2.5	0.02
11		Sand	Pipe (closed)	Steel	6.1	73	12	11.16	0.07
12		Sand	Pipe (closed)	Steel	6.1	88.9	12	11.16	0.07
13		Sand	Pipe (closed)	Steel	6.1	114.3	12	11.16	0.07
14		Sand	Pipe (open)	Steel	6.1	73	12	11.16	0.07
15		Sand	Pipe (open)	Steel	6.1	88.9	12	11.16	0.07
16	[26]	Sand	Round	Concrete	16	280	3.2	3.38	0.02
17	[27]	Sand	Pipe (closed)	Steel	8.24	356	3	11.1	0.07
18		Sand	Pipe (open)	Steel	8.24	356	3	17.65	0.17
19	[28]	Sand	Pipe (closed)	Steel	3.5	73	6	15.6	0.11
20		Sand	Pipe (closed)	Steel	3.44	73	6	15.6	0.11
21	[29]	Sand	Square	Concrete	6	350	11	3.38	0.02
22	[30]	Sand	Square	Concrete	11	253	6.2	38	1
23		Sand	Square	Concrete	15	253	6	49	1.27
24		Sand	Octagonal	Concrete	19.5	610	1	37	0.16
25		Sand	Round	Concrete	8	280	1.7	25	0.1
26		Sand	Round	Concrete	16	280	1.7	32	0.13
27		Sand	Round	Concrete	7.5	280	1.7	21	0.08
28		Sand	Round	Concrete	11.5	280	1.7	27	0.11
29		Sand	Round	Concrete	15.5	280	1.7	32	0.125
30		Sand	Square	Concrete	12.8	235	2	39	0.17
31		Sand	Square	Concrete	15.2	406	1.5	112	0.28
32		Sand	Square	Concrete	32	610	1	24	0.19
33		Sand	Round	Steel	19	660	1	39	0.17
34		Sand	Round	Steel	6.8	356	3.2	388	3.34
35		Sand	Round	Steel	6.1	457	1.5	111	0.42
36		Sand	Round	Steel	6.9	356	1.5	190	1.05
37		Sand	Round	Steel	11	813	3	29	0.17
38		Sand	Round	Concrete	19.5	280	1.7	50	0.21
39		Sand	Round	Concrete	23.5	280	1.7	62	0.25
40		Sand	Square	Concrete	16.8	235	1.3	112	0.49

L pile length, b pile diameter, $G.W.T.$ ground water table, q_c the geometric average of cone tip resistance in a zone extended from $4b$ below the cone tip to $8b$ above the tip, f_s the geometric average of cone sleeve friction over pile length

considered in this study by defining the progressive soil friction angle as an input data in numerical modeling and the stress characteristics network is updated in each step. In Fig. 2, the stress fields around the pile is illustrated for initial yield condition and the failure mechanism.

Studies show that the size of failure mechanism obtained by the stress characteristics method through initial yield to

failure condition does not change perceptibly (as shown in Fig. 2). Therefore, it is assumed that the failure pattern found by a stress field at limiting equilibrium remains stationary along sliding discontinuities. This simplification can alternatively be used to reduce the computational effort.

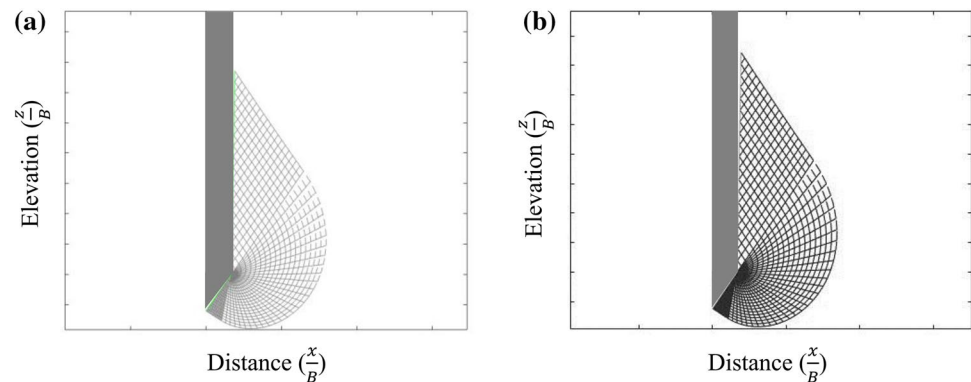
The obtained failure pattern is then used to calculate the kinematics of progressing failure, i.e., the displacement

Table 3 Case study records for verification

No.	Refs.	Soil type	Pile shape	Material	L (m)	b (mm)	G.W.T (m)	q_c (MPa)	f_s (MPa)
1	[24]	Sand	Pipe (closed)	Steel	10.02	457	4	1.89	0.02
2		Sand	Pipe (closed)	Steel	10	457	4	1.91	0.01
3		Sand	Pipe (closed)	Steel	19.32	457	4	1.74	0.01
4		Sand	Pipe (closed)	Steel	18.85	457	4	1.83	0.01
5	[30]	Sand	Square	Concrete	17.8	235	1.3	144	0.66
6		Sand	Square	Concrete	16.2	275	1.3	78	0.34
7		Sand	Square	Concrete	25.9	610	1	11	0.09
8		Sand	Round	Steel	9.2	273	2.5	63	0.17
9		Sand	Round	Steel	8.9	457	1.5	118	0.39
10		Sand	Round	Steel	12	457	1.5	83	0.27
11		Sand	Round	Steel	15	457	1.5	102	0.26
12		Sand	Round	Steel	14.2	305	0	167	0.63
13		Sand	Round	Steel	14.4	356	0	155	0.59
14		Sand	Round	Steel	14.6	406	0	145	0.54
15		Sand	Round	Steel	13.3	610	0	96	1.47
16		Sand	Round	Steel	15	813	3	53	0.22
17		Sand	Round	Steel	25	813	3	32	0.21
18		Sand	Round	Steel	10	457	4	244	2.07
19		Sand	Round	Steel	30.5	763	1	307	3.75
20		Sand	Round	Steel	38.7	763	1	231	3.3
21		Sand	Round	Steel	47	763	1	230	3.04
22		Sand	Round	Steel	46.7	763	1	230	3.54
23	[31]	Sand	Square	Concrete	14	450	0	9.11	0.11
24		Sand	Pipe (closed)	Steel	18.2	660	2	9.31	0.05
25		Silt	Pipe (open)	Steel	67	915	2	3.74	0.04
26		Hydraulic sand	Pipe (closed)	Steel	9.2	273	2.5	5.03	0.02
27		Uniform sand	Square	Concrete	11	285	6	4.18	0.1
28		Uniform sand	Square	Concrete	15	285	6	5.51	0.11
29		Sand	Octagonal	Concrete	25.8	600	4	6.23	0.1
30		Sand	Pipe (closed)	Steel	34.25	609	1	2.35	0.07
31		Sand	Pipe (closed)	Steel	34.25	609	1	9.08	0.1
32		Sand	Square	Concrete	16	350	0	5.89	0.14
33		Sand	Square	Concrete	11	500	0	11.98	0.05
34		Silt	Square	Concrete	20.4	350	0	4.84	0.18
35		Sand	Round	Concrete	18.2	610	2	8.92	0.05
36		Sand	Pipe (closed)	Steel	16.2	300	0	14.74	0.08
37		Sand	Pipe (closed)	Steel	14.4	350	0	14.74	0.08
38		Sand	Pipe (closed)	Steel	14.6	400	0	14.74	0.08
39		Sand	Pipe (closed)	Steel	11.1	350	0	14.74	0.08
40		Sand	Pipe (closed)	Steel	11	300	0	14.74	0.08
41		Sand	Square	Concrete	10.2	355	0	4.74	0.06
42		Silty sand	Square	Concrete	8	450	0	3.73	0.06
43		Silty sand	Square	Concrete	11.3	450	0	2.6	0.04
44		Sand	Square	Concrete	9.15	450	0	10.52	0.24

Table 3 (continued)

No.	Refs.	Soil type	Pile shape	Material	L (m)	b (mm)	G.W.T (m)	q_c (MPa)	f_s (MPa)
45		Sand	Square	Concrete	21.3	250	0	5.09	0.06
46		Silty sand	Square	Concrete	15.85	350	0	5.92	0.09
47		Loose sand	Pipe (closed)	Steel	15.2	273	0	8.02	0.08
48		Sand	Pipe (closed)	Steel	22.5	273	0	7.73	0.09
49		Sand	Square	Concrete	14.9	450	0	6.54	0.07
50		Sand	Square	Concrete	8.6	350	0	4.78	0.06
51		Sand	Square	Concrete	15	450	0	6.09	0.11
52		Sand	Square	Concrete	11.3	400	0	5.84	0.19
53		Sand	Square	Concrete	16	350	0	6.74	0.15
54		Sand	Square	Concrete	11.4	400	0	6.43	0.16
55		Sand	Square	Concrete	11.2	400	0	7.87	0.15
56		Sand	Square	Concrete	12.5	400	0	3.81	0.07
57		Sand	Square	Concrete	25	350	0	6.08	0.1
58	[32]	Sand	Square	Concrete	19.1	235	2	4.88	0.01

Fig. 2 Stress field formed around the pile for **a** initial yield condition and **b** failure condition

field for a given displacement boundary. In the incremental load–displacement computation procedure, the incremental displacement field is constructed at each step and then the strain field will be obtained. The mobilized soil friction angle is a function of the shear strain and hence, at each step, the associated stress field is updated in accordance with the incremental displacement field. Thus, the stress characteristics network and the failure mechanism are updated in every step according to the displacement field and the mobilized friction angle. In the next section, the calculation of the displacement field is described.

4.2 Kinematics of Deformation and Displacement Field

In this section, the general outline of the procedure to find the displacement fields is presented. It is divided into two sections for the pile tip and the shaft, respectively. As stated in former section, the construction of the displacement field and the associated stress field is a progressive and incremental computation. In each step, the incremental displacement field is calculated, the shear strain increment is found

and based on the shear strain, the mobilized friction angle and finally, the associated stress field at that particular step is calculated. In what comes next, the construction of the incremental displacement field is explained for the pile tip and the shaft.

4.2.1 Pile Tip

Once the stress state at every point around the pile has been computed using the slip lines equations, an admissible velocity field can be found corresponding to the failure mechanism already obtained by the stress characteristics. In other words, the stress characteristics network designates the extent of the failure mechanics and this failure mechanism can be then used to construct the displacement field. Construction of displacement field (in fact, the displacement increment or the velocity, in the terminology of the limit analysis) is done by making the velocity hodographs corresponding to the velocities of different rigid blocks enclosed by slip lines. One should note that the stress characteristics network defines the directions of slip and hence, the soil block enclosed by these lines, can be regarded as a rigid

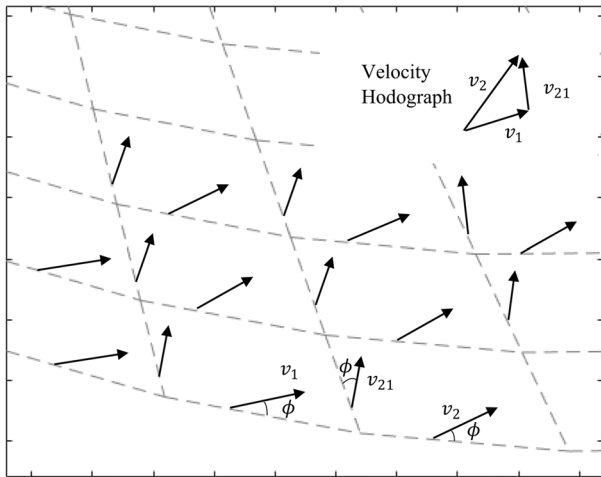


Fig. 3 Velocity hodographs and rigid blocks

block. In fact, deformations are highly localized into the slip lines and in the exterior of the slip lines, deformations are elastic, or, even zero in case of a rigid-perfectly plastic material. This approach is recently presented and described in detail, by Veiskarami et al. [14] and applied to estimate the bearing capacity of strip foundations [15].

Figure 3 shows the failure pattern (obtained by the method of stress characteristics) and the velocity vectors acting on the slip lines. In associated flow rule condition, the stress characteristics lines coincide with the zero extension lines (i.e., lines of zero axial strains) and therefore, the slip lines can be considered as rigid links that can move or rotate without axial deformation. For non-associated flow rule, the procedure outlined in Sect. 2.3 can be utilized to arrive at an equivalent associated flow rule condition. Now, for a given deformation boundary condition, the generated displacements in the network can be computed by the following equation:

$$\frac{du}{dv} = -\frac{dz}{dx} \tag{8}$$

In this equation, u and v are horizontal and vertical displacements. The finite difference forms of these equations can be used to find the displacement field for further computations which are presented in Eqs. 9 and 10:

$$du \, dx + dv \, dz = 0, \tag{9}$$

$$\begin{cases} (u_{B2} - u_{A2})(x_{B2} - x_{A2}) + (v_{B2} - v_{A2})(z_{B2} - z_{A2}) = 0 \\ (u_{B2} - u_{A3})(x_{B2} - x_{A3}) + (v_{B2} - v_{A3})(z_{B2} - z_{A3}) = 0 \end{cases} \tag{10}$$

When the velocity field has been found, the maximum shear strains can be determined, which is presented below:

$$\gamma = \frac{\partial u}{\partial z} + \frac{\partial v}{\partial x} \tag{11}$$

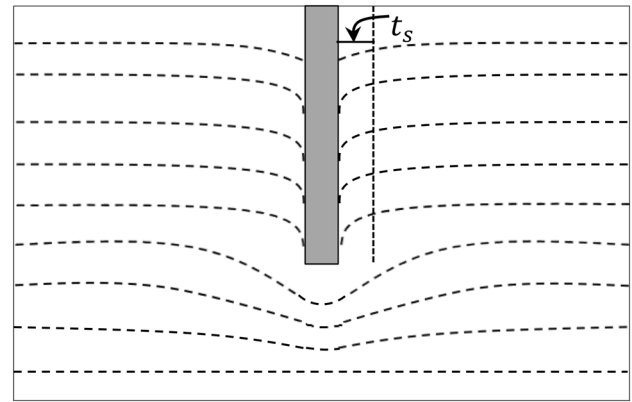


Fig. 4 Shear pattern around pile in sand

The incremental displacement field can be obtained by incremental boundary displacement. In this case, the incremental boundary displacement is nothing but the vertical movement of the pile tip into the ground.

4.2.2 Pile Shaft

The same procedure should be taken for the pile shaft, i.e., the displacement field and the progressive failure pattern around the pile shaft in an incremental manner. As it is shown in Fig. 4, there is a sheared region (also called the smear zone) around the pile shaft in granular soils with a vertically aligned stretching [33]. The mobilization and ultimate value of the shaft friction is governed by the behavior of this narrow zone in the proximity of the pile surface [34]. Previous model tests have shown that the soil located far enough from the shaft remains largely undeformed [35]. A survey in the literature shows that the thickness of this shear zone, t_s , depends on the pile surface roughness and has a very wide range [36, 37]. A summary of these investigations on the thickness of the shear zone is shown in Table 4. According to this table, t_s , for this study, is assumed to be $10D_{50}$ for sand as an average value of what has been suggested by researchers.

In Fig. 5, the behavior of the shear zone during installation and static loading is shown. The shear displacement, δ ,

Table 4 The thickness of shear (or smear) zone around pile shaft

No.	References	Equation	Remarks
1	[34]	$t_s = (2 - 5)D_{50}$ $t_s = (10 - 15)D_{50}$	Smooth pile Rough pile
2	[36, 37]	$t_s = 3.5 - 5.5 \text{ mm}$	Silica sand

D_{50} mean particle size of the sand

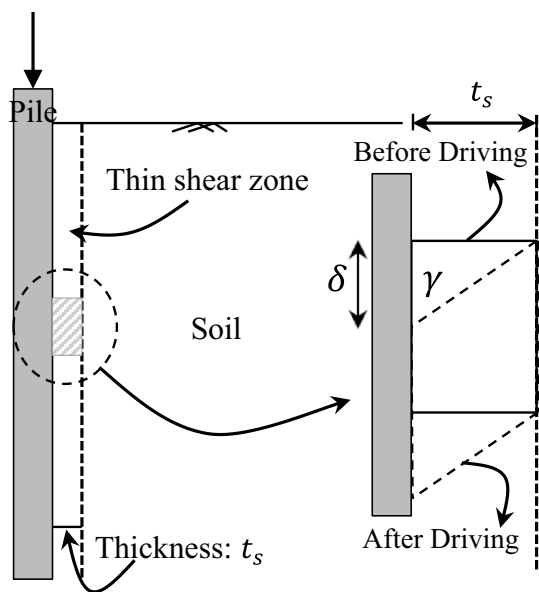


Fig. 5 Behavior of the shear (or the smear) zone during installation and loading

leads to mobilization of shaft capacity of pile. Therefore, the shear strain can be obtained by Eq. 12 as follows:

$$\gamma = \frac{\delta}{t_s} \tag{12}$$

The pile unit shaft resistance, r_s , may be determined from the sleeve friction as expressed by:

$$r_s = Kf_s \tag{13}$$

where K is a dimensionless coefficient. The K coefficient depends on the pile shape and its material, cone type and embedment ratio. In sand, the coefficient, K , ranges between 0.8 and 2 [38, 39].

5 CPT-Based Load–Displacement Curve for Piles

The numerical procedure has been developed as presented to obtain the stress and strain fields around the pile. Now, it is necessary to consider an appropriate constitutive model to study the load–displacement behavior of the piles. This is possible by studying the relationship between $\sin \phi_{mob.}$ and γ_{max} in each element of the soil obtained from the presented numerical modeling of the stress and strain field around the pile.

The mobilized soil friction angle and the maximum shear strain are functionally dependent. This functional relationship is highly important and very influential in stress analysis when the displacement field is prescribed. Unfortunately, an explicit and clear form of such equation has not been found by the authors in the literature. However, a very simple form of such a functional dependency can be found by assuming a hyperbolic relationship between $\sin \phi_{mob.}$ and the maximum shear strain. This form can be visually supported by the form of conventional shear tests on frictional soils, e.g., [40, 41] and also, supported by the form of hardening laws presented by traditional soil models such as the hyperbolic soil model, e.g., [42, 43]. In addition, such an equation is not only capable of qualitative capturing of the soil behavior, but also requires the minimum number of parameters (only two) to be prescribed [44]. Therefore, the following equation has been chosen as a basis for the functional dependency of the mobilized friction angle and the maximum shear strain depicted graphically in Fig. 6a:

$$\sin \phi_{mob.} = \frac{\gamma}{a + b\gamma} \tag{14}$$

In this equation, two parameters of a and b can be considered as representatives of the geotechnical (or mechanical) parameters, i.e., the modulus of elasticity, E and the critical state (or the residual) friction angle, $\phi_{c.s.}$. For instance, a is some measure of E and $b = 1/\sin \phi_{c.s.}$.

This hyperbolic relation is assumed to define the progressive soil friction angle and updated stress and strain field

Fig. 6 **a** Hyperbolic relation between $\sin \phi_{mob.}$ and maximum shear strain, **b** general form of predicted hyperbolic load transfer for each element of soil around the pile

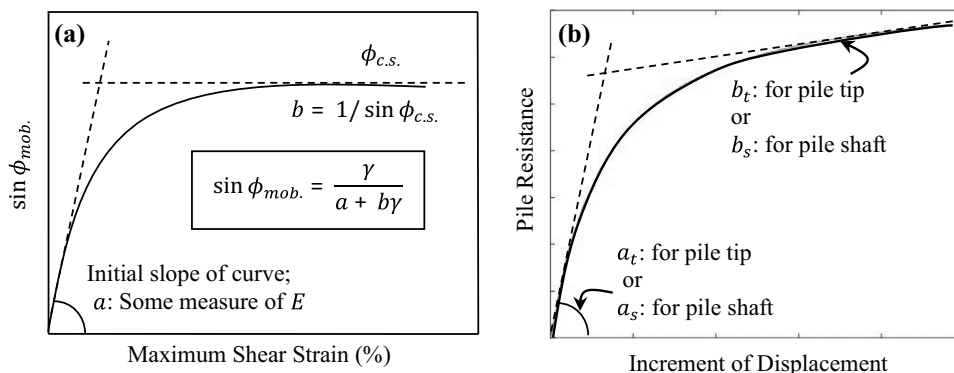


Fig. 7 The input parameters of load–displacement curve for pile tip

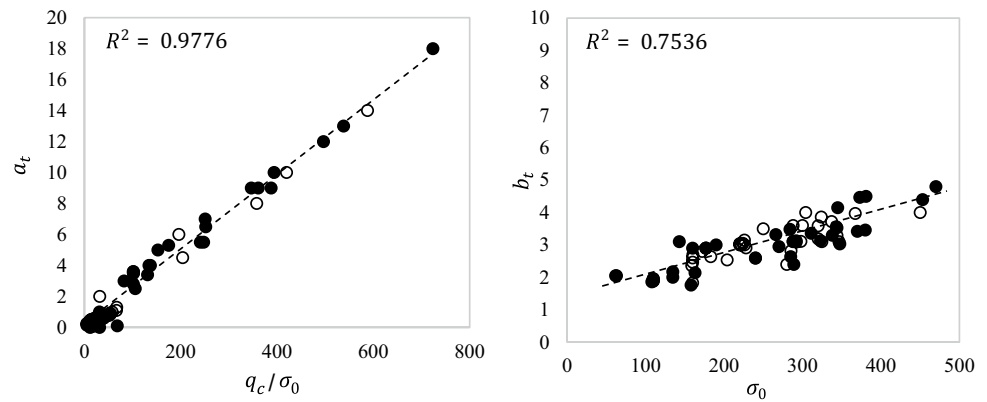
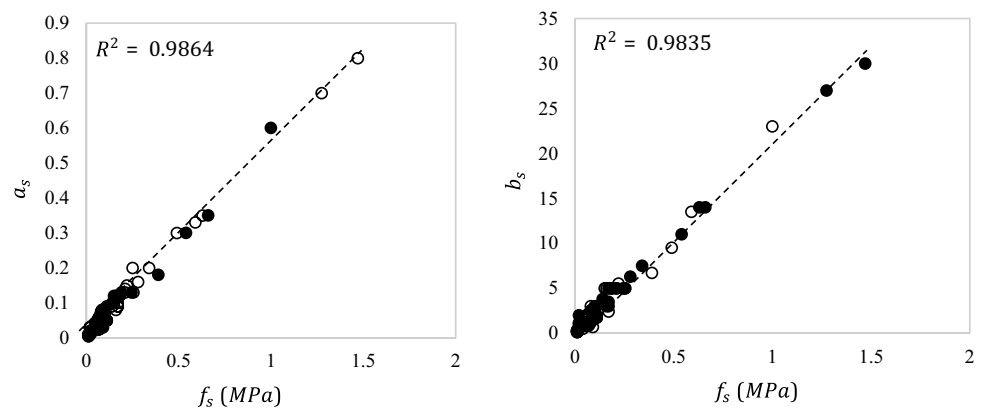


Fig. 8 The input parameters of load–displacement curve for pile shaft



formed around the pile. This procedure continuous until the soil fails. Therefore, in each step, stress–strain response in every element of the soil obeys the same hyperbolic trend. The response of the soil for each increment of displacement as an output of numerical study is presented in Fig. 6b. Now, this local trend in soil elements could be generalized reasonably to load–displacement response of the pile under axial loading.

It is worth mentioning that, although Eq. 14 is not basically for layered soils as well as a soil with varying properties in depth, the non-homogeneity of the soil can be considered by use of CPT data in the proposed approach. As described in Sect. 2.4, the soil properties in different layers are obtained using CPT data, which reflect a continues (inch-by-inch) actual properties of the soil. Therefore, it can be said that, as the model parameters are linked to the corresponding CPT data at that particular depth, the non-homogeneity of the soil can be automatically considered.

This study shows that the input parameters required for load transfer (hyperbolic) curves have physical meaning and determined from analysis of proposed stress and strain fields formed around the pile. To calibrate the model parameters, 40 case studies (for which there was a complete database available), presented in Table 2, were used. The rest of case studies,

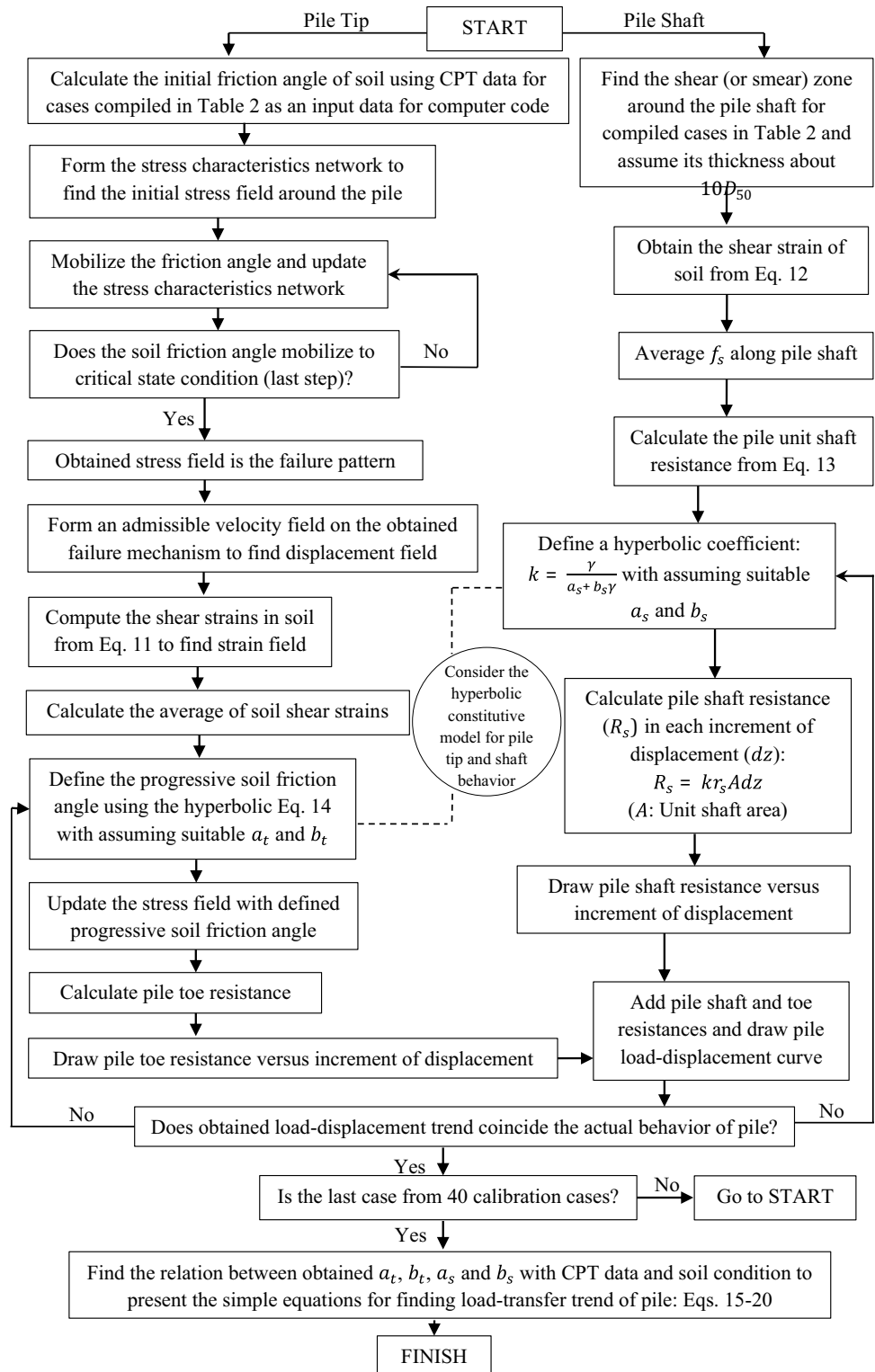
presented in Table 3, were used to verify the calibrated parameters. Inspection of the results revealed that the input parameters for pile tip and shaft are functions of the ratio q_c/σ_0 , σ_0 and f_s where σ_0 is the initial soil pressure at the depth at which, these curves are required. This dependency seems to be logical as the stress level effect cannot be disregarded. However, the effect of pile geometry such an effect could not be well-recognized in this paper due to the rather tight range of pile dimensions in available collected database. The input parameters for the pile tip load transfer (hyperbolic) curve are shown in Fig. 7 with equations obtained below. In these equations, q is the effective overburden pressure of soil at pile tip, t is shear stress at the pile shaft and ζ is vertical movement of the pile:

$$q = \frac{\zeta}{a_t + b_t \zeta}, \quad (15)$$

$$a_t = 0.03 \left(\frac{q_c}{\sigma_0} \right) + 0.012, \quad (16)$$

$$b_t = 0.006 \sigma_0 + 1.39. \quad (17)$$

Fig. 9 Flowchart to summarize proposed approach



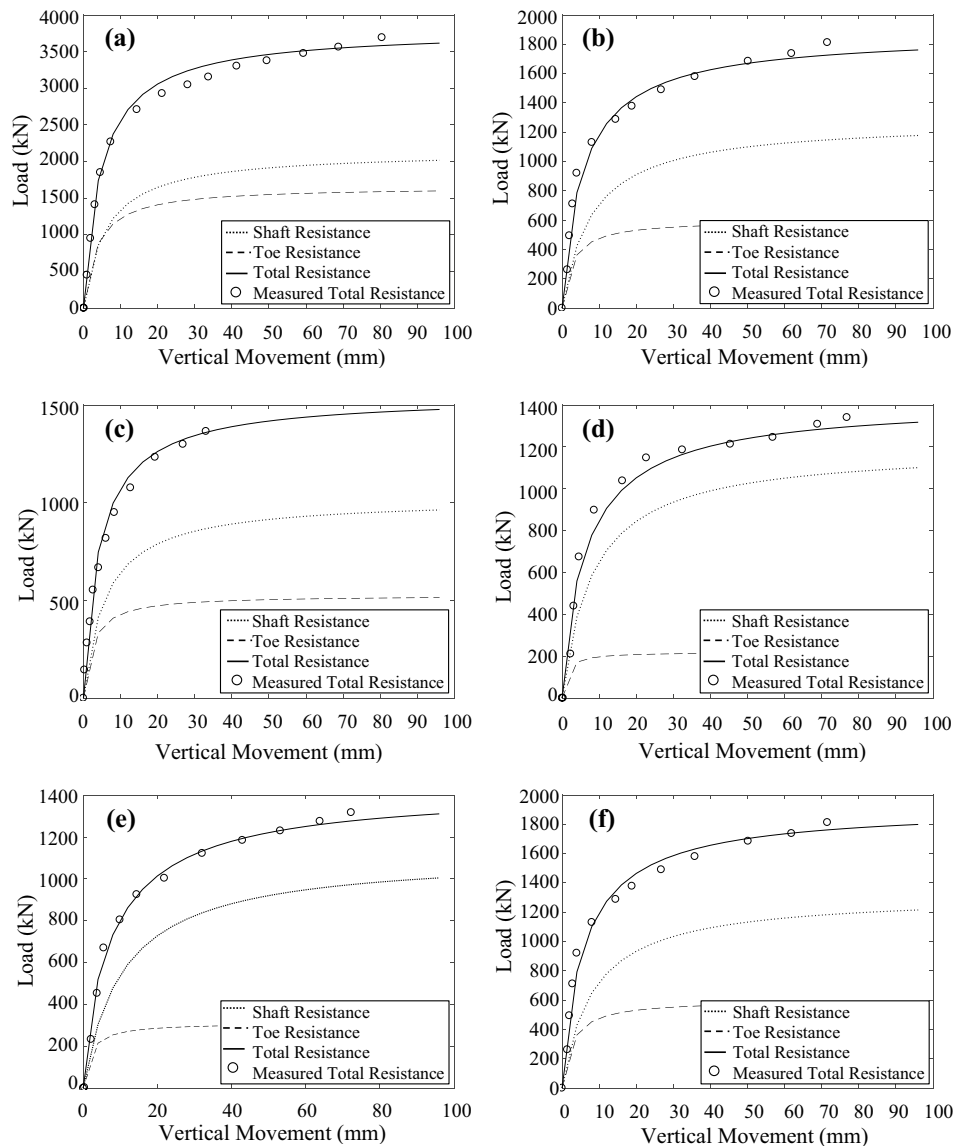
A similar analytical approach has been conducted for the parameters of the shaft load transfer curve with the results shown in Fig. 8 and parameters presented below:

$$t = \frac{\zeta}{a_s + b_s \zeta}, \tag{18}$$

$$a_s = 0.55 (f_s) + 0.01, \tag{19}$$

$$b_s = 21 f_s + 0.21. \tag{20}$$

Fig. 10 Predicted load–displacement responses of selected piles using proposed approach: **a** Case 24, **b** Case 27, **c** Case 32, **d** Case 36, **e** Case 37 and **f** Case 38 (from Table 3)



Both the calibration and verification data points are shown in Figs. 7 and 8 separated by different notations (circles with solid fill or no fill, respectively). It is apparent that the linear predictions are suitable and show reasonable agreement.

The flowchart of the developed procedure is shown in Fig. 9 to clarify the proposed approach step-by-step.

6 Load–Displacement Results

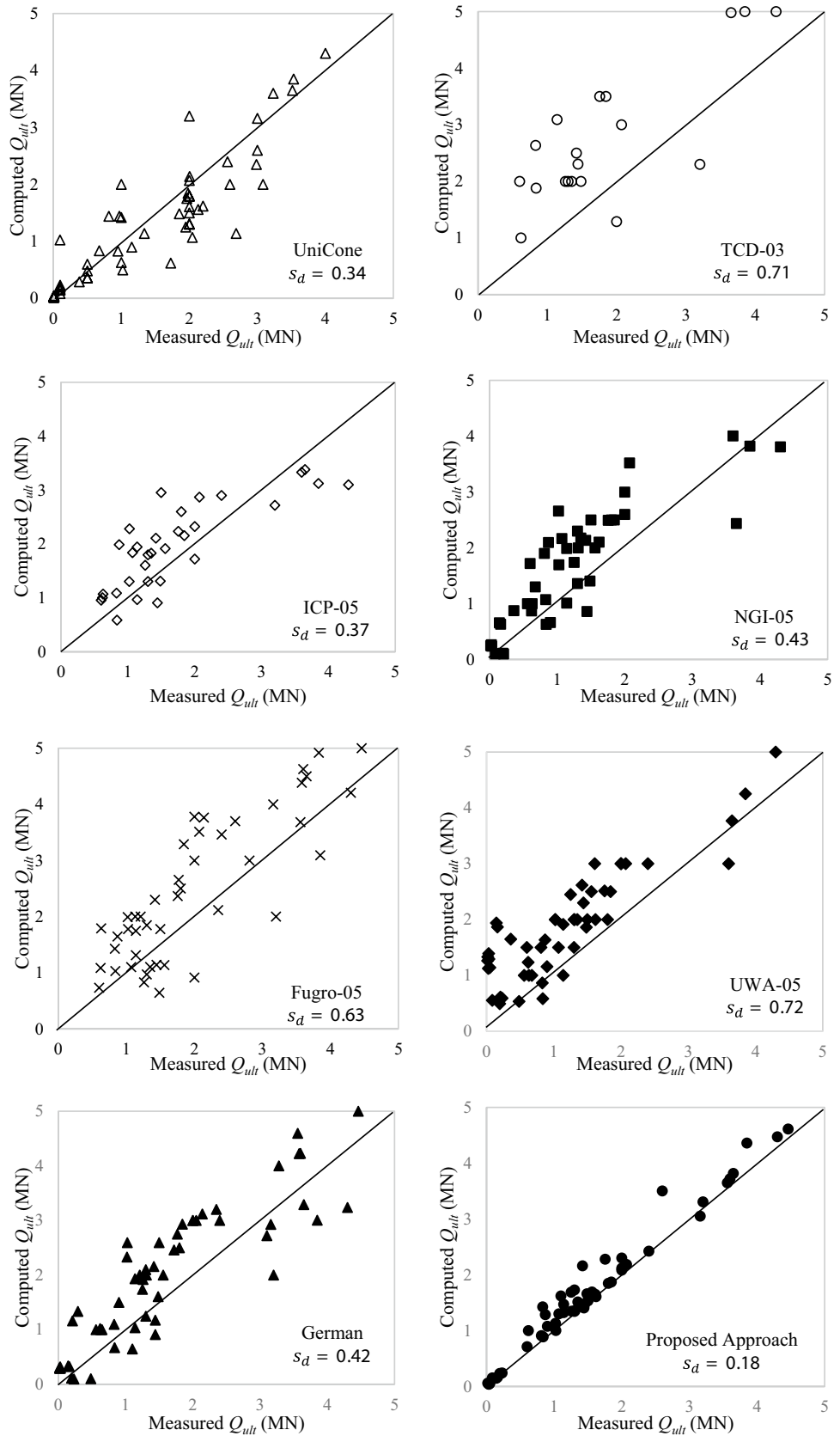
The results of the numerical modeling of the load–displacement response of the proposed procedure for some arbitrary case studies from Table 3 are shown in Fig. 10. The responses to the toe and shaft resistances are separately presented and the overall response is compared with that, obtained by field tests. The accuracy of the predicted

load–displacement responses is clear. It is worth mentioning that for cases no. 7, no. 11, no. 20 and no. 21, in Table 3, predictions showed less agreement with observed responses. This can be attributed to the inaccuracy of the empirical relationships between CPT results and soil shear strength parameters. Fortunately, the agreement between predictions and observations in the rest of case studies was quite reasonable and similar to those corresponding to cases shown in Fig. 10.

7 Pile Bearing Capacity by Proposed Approach

To compare the results of the proposed method by other methods, the bearing capacity of 58 cases used for verification reported in Table 3 are estimated by the proposed

Fig. 11 Estimated versus measured bearing capacity of piles by different CPT-based methods



approach and also other CPT-based methods. For this purpose, seven methods were used comprising: UniCone [31], TCD-03 [45], ICP-05 [46], NGI-05 [47], Fugro-05 [48], UWA-05 [49], German [50]. The results are presented in Fig. 11. It is worth mentioning that in this study, the plunging failure is taken as the ultimate bearing capacity of the piles, since the bearing capacity of pile is estimated based on CPT, which is a large strain test. Furthermore, the Brinch Hansen 80%-criterion [51] is used for the cases that the failure load is not clearly defined. Since the 80%-criterion normally agrees well with the intuitively perceived plunging of the pile [52], it can be observed that the proposed approach provides fairly better predictions rather than the other ones.

8 Conclusions

Based on the principles of the plasticity theory, the stress field is not independent of the displacement and/or deformation fields. Therefore, a more reliable analysis will be achieved if the bearing capacity and load–displacement behavior of piles are analyzed simultaneously.

The main objective of this paper is to propose a method to predict the load–displacement behavior and the bearing capacity of driven piles in sand. A new analytical–numerical method has been proposed to estimate the bearing capacity and axial load–displacement behavior of driven piles using CPT records.

For this purpose, the method of stress characteristics is employed to analyze the stress field below and around the pile. Furthermore, the load–displacement behavior of piles is studied by the implementation of a displacement field on the current actual stress field obtained by the stress characteristics method. The geotechnical parameters required for numerical analyses are obtained from in situ tests. To do this, the CPT data has been both directly and indirectly incorporated into the analyses to estimate the soil shear strength parameters and the bearing capacity of piles. A simple hyperbolic relationship has been introduced to relate the shear strain and the mobilized shear resistance of soil in terms of the mobilized friction angle. The procedure comprises some steps through which, the load–displacement and bearing capacity of driven piles can be obtained.

To calibrate the load–displacement hyperbolic relationship, a rather large pile load test database, including 98 driven piles in sand, has been recompiled with CPT data available. Pile materials are concrete or steel and the shapes of piles are octagonal, square, round and pipe (opened and closed ended). The pile width and length vary between 73–915 mm and 3.44–67 m, respectively. Calibration of the parameters has been made first for 40 case histories and then, it is verified for the remaining of the pile load test data.

Finally, the axial pile bearing capacity estimated by the proposed method is compared by the results obtained by seven direct CPT-based methods. Comparisons showed that this proposed approach is capable of promoting accuracy and the predictions are in acceptable agreement with full-scale pile load tests results. The reason may lie behind the fact that the proposed approach integrates several ingredients of the plasticity theory and limit analysis, direct and indirect use of the CPT results, i.e., a theoretical approach on the basis of a rather accurate and continuous record of the soil properties. Of course, the accuracy of the proposed approach mainly depends on the type of the conducted in situ test. In addition, in this study, the bearing capacity is estimated considering the displacements occurred in the soil, which has not been concerned in the other common CPT-based methods. As far as the CPT data are available and representing the actual subsoil condition, the proposed approach can be a good alternative among other methods for the load–displacement as well as the bearing capacity analysis of driven piles.

References

1. CFEM (2012) Canadian foundation engineering manual, 4th edn. Canadian Geotechnical Society, Vancouver
2. Fellenius BH (2018) Basics of foundation design—a textbook. Electronic Edition, p 451. <http://www.Fellenius.net>
3. Fellenius BH (1988) Unified design of piles and pile groups. Transportation Research Board, TRB Record 1169, Washington D.C, pp 75–82
4. Chen JJ, Zhang L (2013) Effect of spatial correlation of cone tip resistance on the bearing capacity of piles. *J Geotech Geoenviron ASCE* 139:494–500
5. Moshfeghi S, Eslami A (2016) Study on pile ultimate capacity criteria and CPT-based direct methods. *Int J Geotech Eng* 12:28–39
6. Bazar MH, Kashkooli A, Saeedi-Azizkandi A (2012) Prediction of pile shaft resistance using cone penetration tests (CPTs). *Comput Geotech* 45:74–82
7. Eslami A, Valikhah F, Veiskarami M, Salehi M (2017) CPT-based investigation for pile toe and shaft resistances distribution. *Geotech Geol Eng* 13:2891–2905
8. Battaglio M, Jamiolkowski M, Lancellotta R, Maniscalco R (1981) Piezometer probe test in cohesive deposits. In: ASCE, geotechnical division, symposium on cone penetration testing and experience, pp 264–302
9. Robertson PK, Campanella RG (1983) Interpretation of cone penetration tests. Part I: sand. *Can. Geotech J* 20:718–733
10. Sokolovski VV (1960) Statics of soil media (Translated by D.H. Morton-Jones and A.N. Schofield). Butterworths, London, p 237
11. Martin CM, Houlsby GT (2001) Combined loading of spudcan foundations on clay: numerical modeling. *Géotechnique* 51:687–699
12. Kumar J (2009) The variation of with footing roughness using the method of characteristics. *Int J Numer Anal Methods Geomech* 33:275–284
13. Veiskarami M, Eslami A, Kumar J (2011) End bearing capacity of driven piles in sand using the stress characteristics method: analysis and implementation. *Can Geotech J* 48:1570–1586
14. Veiskarami M, Kumar J, Valikhah F (2014) Effect of the flow rule on the bearing capacity of strip foundations on sand by the

- upper-bound limit analysis and slip lines. *Int J Geomech ASCE*, [https://doi.org/10.1061/\(ASCE\)GM.1943-5622.0000324](https://doi.org/10.1061/(ASCE)GM.1943-5622.0000324)
15. Veiskarami M, Kumar J, Valikhah F (2015) A practical procedure to estimate the bearing capacity of footings on sand—application to 87 case studies. *IJSTC Trans Civ Eng* 39(C2⁺):469–483
 16. Bolton MD, Lau CK (1993) Vertical bearing capacity factors for circular and strip footings on Mohr–Coulomb soil. *Can Geotech J* 30:1024–1033
 17. Veiskarami M, Zanj A (2014) Stability of sheet-pile walls subjected to seepage flow by slip lines and finite elements. *Géotechnique* 64(10):759–775. <https://doi.org/10.1680/geot.14.P.020>
 18. Larkin LA (1968) Theoretical bearing capacity of very shallow footings. *J Soil Mech Founda Div (ASCE)* 94(6):1347–1360
 19. Drescher A, Detournay E (1993) Limit load in translational failure mechanisms for associative and non-associative materials. *Géotechnique* 43:443–456
 20. Davis EH (1968) Theories of plasticity and the failure of soil masses. In: Lee IK (ed) *Soil mechanics: selected topics*. Butterworth & Co Publishers Ltd., London, pp 341–380
 21. Rowe PW (1969) The relation between the shear strength of sands in triaxial compression, plane strain and direct shear. *Géotechnique* 19:75–86
 22. Bowles JE (1996) *Foundation analysis and design*, 5th edn. The McGraw-Hill Companies, Inc., New York
 23. Kulhawy FH, Mayne PW (1990) *Manual on estimating soil properties for foundation design*, Electric Power Research Institute EL-6800, Project 1493-6. Electric Power Research Institute, Palo Alto
 24. Jardine RJ, Standing JR (2000) Pile load testing performed for HSE cyclic loading study at Dunkirk, France. *Offshore Technology Report OTO 2000 007*, vol 2. Health and Safety Executive, London, p 60, 200
 25. Lutenecker AJ, Kelley SP (2000) Tension tests on driven piles in sand. In: *Proceedings of 8th international conference on deep foundations*, pp 219–225
 26. Fellenius BH (2002) Determining the true distribution of load in piles. In: O'Neill MW, Townsend FC (eds) *International deep foundation congress, an international perspective on theory, design, construction, and performance*, ASCE, GSP116, Orlando, February 14–16, 2002, vol 2, pp 1455–1470
 27. Paik K, Salgado R, Lee J, Kim B (2003) Behavior of open- and closed-ended piles driven into sands. *J Geotech Geoenviron Eng ASCE* 129:296–306
 28. Gavin KG, O'Kelly BC (2007) Effect of friction fatigue on pile capacity in dense sand. *J Geotech Geoenviron Eng ASCE* 133:63–71
 29. Fellenius BH, Santos JA, Fonseca AVD (2007) Analysis of piles in a residual soil—the ISC² prediction. *Can Geotech J* 44:201–220
 30. Schneider JA, Xu X, Lehane BM (2008) Database assessment of CPT-based design methods for axial capacity of driven piles in siliceous sands. *J Geotech Geoenviron ASCE* 134:1227–1244
 31. Eslami A, Fellenius BH (1997) Pile capacity by direct CPT and CPTu methods applied to 102 case histories. *Can Geotech J* 34:886–904
 32. Axelsson G (1998) Long-term increase in shaft capacity of driven piles in sand. In: *Proceedings 4th international conference on case histories in geotechnical engineering*, St. Louis, March 9–12, 1998
 33. Vesić AS (1967) A study of bearing capacity of deep foundations. Final Report Project B-169. Georgia Institute of Technology, Engineering Experiment Station, Atlanta
 34. Fioravante V (2002) On the shaft friction modeling of non-displacement piles in sand. *Soils Found* 42:23–33
 35. White DJ, Bolton MD (2004) Displacement and strain paths during plane-strain model pile installation. *Géotechnique* 54:375–397
 36. DeJong JT, Randolph MF, White DJ (2003) Interface load transfer degradation during cyclic loading: a microscale investigation. *Soils Found* 43:81–93
 37. Yu F, Yang J (2012) Improved evaluation of interface friction on steel pipe pile in sand. *J Perform Constr Facil* 26:170–179
 38. Nottingham LC (1975) Use of quasi-static friction cone penetrometer data to predict load capacity of displacement piles. PhD thesis. University of Florida, Department of Civil Engineering, Gainesville, p 553
 39. Schmertmann JH (1978) *Guideline for cone penetration test (Performance and design)*. Report No. FHWA-TS-78-209. U.S. Department of Transportation, Washington, DC, p 145
 40. Clark JI (1998) The settlement and bearing capacity of very large foundations on strong soils. 1996 R.M. Hardy Keynote address. *Can Geotech J* 35:131–145
 41. Jahanandish M, Veiskarami M, Ghahramani A (2011) Investigation of foundations behavior by implementation of a developed constitutive soil model in the ZEL method. *Int J Civ Eng* 9(4):293–306
 42. Lade PV, Duncan JM (1975) Elastoplastic stress–strain theory for cohesionless soil. *J Geotech Geoenviron ASCE* 101:1037–1053
 43. Veiskarami M, Mir Tamizdoust M (2017) Bifurcation analysis in sands under true triaxial conditions with coaxial and noncoaxial plastic flow rules. *J Eng Mech ASCE*. [https://doi.org/10.1061/\(ASCE\)EM.1943-7889.0001344](https://doi.org/10.1061/(ASCE)EM.1943-7889.0001344)
 44. Zhang QQ, Li LP, Chen YJ (2014) Analysis of compression pile response using a softening model, a hyperbolic model of skin friction, and a bilinear model of end resistance. *J Eng Mech ASCE* 140:102–111
 45. Gavin KG, Lehane BM (2003) The shaft capacity of pipe piles in sand. *Can Geotech J* 40:36–45
 46. Jardine J, Chow F, Overy R, Standing J (2005) *ICP design methods for driven piles in sands and clays*. Thomas Telford Publishing Ltd., London, p 105
 47. Clausen C, Aas P, Karlsrud K (2005) Bearing capacity of driven piles in sand, the NGI approach. In: *1st international symposium on frontiers in offshore geotechnics, ISFOG 2005, Perth*, pp 677–682
 48. Kolk H, Baaijens A, Senders M (2005) Design criteria for pipe piles in silica sands. In: *1st international symposium on frontiers in offshore geotechnics, ISFOG 2005, Perth*, pp 711–716
 49. Lehane BM, Scheider JA, Xu X (2005) The UWA-05 method for prediction of axial capacity of driven piles in sand. In: *1st international symposium on frontiers in offshore geotechnics, ISFOG 2005, Perth*, pp 683–689
 50. Kempfert HG, Becker P (2010) Axial pile resistance of different pile types based on empirical values. In: *Proceedings of Geo-Shanghai international conference, deep foundations and geotechnical in situ testing*, pp 149–154
 51. Hansen JB (1963) Discussion on hyperbolic stress–strain response, cohesive soils. *J Soil Mech Found Eng (ASCE)* 89(SM4):241–242
 52. Fellenius BH (1995) In: Chen WF (ed) *Geotechnical engineering handbook*. CRC Press, New York